Proceedings of ASME Turbo Expo 2011
GT2011
June 6-10, 2011, Vancouver, British Columbia, Canada

GT2011-46612

OVERALL AND ADIABATIC EFFECTIVENESS VALUES ON A SCALED UP, SIMULATED GAS TURBINE VANE: PART I – EXPERIMENTAL MEASUREMENTS

JASON E. DEES*
The University of Texas at Austin
Austin, Texas USA

DAVID G. BOGARD
The University of Texas at Austin
Austin, Texas USA

GUSTAVO A. LEDEZMA
GE Global Research Center
Niskayuna, NY USA

GREGORY M. LASKOWSKI
GE Global Research Center
Niskayuna, NY USA

ABSTRACT
Recent advances in computational power have made conjugate heat transfer simulations of fully conducting, film cooled turbine components feasible. However, experimental data available with which to validate conjugate heat transfer simulations is limited. This paper presents experimental measurements of external surface temperature on the suction side of a scaled up, fully conducting, cooled gas turbine vane. The experimental model utilizes the matched *Bi* method, which produces non-dimensional surface temperature measurements that are representative of engine conditions. Adiabatic effectiveness values were measured on an identical near adiabatic vane with an identical geometry and cooling configuration. In addition to providing a valuable data set for computational code validation, the data shows the effect of film cooling on the surface temperature of a film cooled part. As expected, in nearly all instances the addition of film cooling was seen to decrease the overall surface temperature. However, due to the effect of film injection causing early boundary layer transition, film cooling at a high momentum flux ratio was shown to actually increase surface temperature over $0.35 < s/C < 0.45$.

INTRODUCTION
In order to keep modern gas turbine airfoils within allowable limits of operating temperature, complicated cooling schemes must be employed. The cooling schemes often consist of a combination of internal convective cooling as well as film cooling on the outer surface of the airfoil. Typically, the analysis of cooled gas turbine airfoils is accomplished through separation of the internal and external cooling configurations via the use of an adiabatic wall. This method has the effect of decoupling the internal and external heat transfer problem. The internal cooling performance can then be characterized in terms of the internal convective heat transfer coefficient. On the external surface, the convective heat transfer coefficient and the adiabatic effectiveness are the primary figures of merit used to evaluate a given film cooling configuration. Decoupling the internal and external problems allows for detailed parametric studies of internal and external cooling designs, however, the value of most interest to designers is the component metal temperature. In order to obtain the component metal temperature, the internal and external heat transfer coefficients as well as the film cooling effectiveness are often supplied to an FEM solver, which then solves for the conduction in the solid metal and the metal temperature. Metal temperatures calculated in this way are only as good as the boundary conditions used in the calculation, which ignore the potential effects of conjugate heat transfer.

Evaluations of the conventional, decoupled analysis methods are very limited in the open literature. The work of Harrison and Bogard [1] used a computational simulation to show that predicted metal temperatures and wall heat fluxes from a fully conjugate calculation disagreed with those calculated using a simulation of conventional analysis techniques. In regions where the conjugate and decoupled

*Currently at GE Global Research Center

predictions disagreed, the authors showed that the gas temperature above the film cooled wall was poorly approximated by the adiabatic wall temperature. The presumption that the adiabatic wall temperature represents the gas temperature immediately above a film cooled part and is the appropriate driving temperature for heat transfer into a film cooled part is an assumption that the decoupled analysis relies on in order to predict the conducting metal temperature.

Recent advances in computational power have allowed for CFD simulations that couple the internal and external flow fields. The great benefit of these simulations is that the metal temperature for a specific cooling configuration can be calculated directly. Validation of CFD models requires well controlled experiments that can quantify boundary conditions. These validated data serve as the foundation for scaling up to engine conditions. Researchers at Aachen University have performed multiple studies highlighting the importance of coupling the internal and external heat transfer [2 – 4]. Additional computational studies detailing conjugate heat transfer on film cooled components, including the effect of *Bi*, are reported in [5 – 7]. Unfortunately, due the limited availability of experimental data, the accuracy of conjugate heat transfer simulations cannot be confirmed.

The work of Hylton et al. [8] details surface temperature measurements at the midspan of a radially cooled metal turbine vane. Showerhead film cooling was added to the geometry of Hylton et al. [8] in the work of Turner et al. [9]. Hylton et al. [10] further expanded the geometry to include pressure side and suction film cooling. In all three studies, midspan external surface temperatures were measured and internal convective heat transfer through the radial cooling channels were calculated using round channel correlations. Additionally, the external heat transfer coefficient was calculated using a finite element method. Despite the limited amount of data, the studies mention previously [8 – 10] became popular as benchmark data for computational simulations primarily due to the lack of any other experimental data on a vane or blade geometry.

Sweeney and Rhodes [11] developed a matched *Bi* model in order to simulate the overall cooling performance of Lamilloy, which uses effusion cooling and a double wall with extensive internal cooling. Sweeney and Rhodes used a flat plate that was constructed of a lower thermal conductivity material (relative to the engine) selected to match *Bi* to engine conditions. Matching *Bi* ensured that the ratio of convective heat transfer at the solid surface to the conduction through the solid matched the engine condition. This allowed for direct measurement of non-dimensional metal temperatures that were representative of an engine component.

Albert et al. [12] used the matched *Bi* model to study a scaled up, film cooled simulated blade leading edge with internal impingement cooling. This study used three rows of shaped film cooling holes around the blade leading edge and measured the overall effectiveness of the cooling configuration. Overall effectiveness measurements combine the effects of internal cooling, external cooling, and conduction in the solid through the use of a conducting wall. Overall effectiveness uses the same equation as adiabatic effectiveness, however; a material with relatively high thermal conductivity is used to construct the model. An adiabatic model with the same geometry was also tested. The main difference seen when comparing the conducting and adiabatic models was a general “smoothing out” of temperature gradients for the case of the conducting model, due to the lateral conduction in the solid model. Spatial variations in overall effectiveness were still present, but were much less severe than the variations seen in the adiabatic effectiveness measurements.

An additional study on the same geometry, by Mouzon et. al. [13], calculated the net heat flux reduction (NHFR) on an adiabatic leading edge and overall effectiveness on a matched *Bi* leading edge and compared them directly. The net heat flux reduction is a measure of the reduction (or augmentation) in heat flux into a component due to the presence of film cooling. The results of the study showed that while trends in NHFR and overall effectiveness were similar, local variations in NHFR were greater than those seen in overall effectiveness. This was attributed to the conducting model having the effect of smoothing out temperature gradients due to lateral conduction.

More recently, the work of Dees et al. [14 – 16] studied a scaled up, matched *Bi* vane cooled with an internal cooling circuit designed to be representative of typical internal cooling configurations. The first study [14] provides detailed surface temperature measurements over the entire vane surface as well as internal surface temperature measurements at select locations. A range of internal coolant flow rates was tested. The second study by Dees et al., [15], presented measurements of the external surface temperature distribution for the same airfoil used in [14], except with rib turbulators installed on the internal suction surface of the vane. The installation of a very common rib turbulator geometry, designed using correlations with the intent of augmenting internal heat transfer by two times, caused as much as a 40% increase in overall effectiveness. Dees et al [16] further expanded the experimental data set by measuring the developing thermal and momentum boundary layers around the internally cooled vane. Since the experimental model matched *Bi* to engine conditions and the non-dimensional surface temperature to engine conditions, the thermal boundary layer development was therefore also representative of engine conditions.

As noted previously, a key limitation in the use of CFD codes for conjugate heat transfer studies is the lack of quality experimental data with which to validate computational codes. An important goal of the current work, in addition to the work of Dees et al. [14 – 16], was to provide an experimental data set for a conducting turbine airfoil that surpasses the current experimental benchmark. Engine test rigs, which automatically match engine conditions, do not provide the detail that can be achieved in a large scale facility. The other experimental studies either did not provide engine representative non-dimensional surface temperatures ([8 – 10]) or were studies of partial components ([11 – 13]). The current study presents detailed surface temperature measurements on identical film cooled conducting and adiabatic turbine vanes. The conducting turbine vane employs the matched Bi method in order to provide engine representative overall effectiveness measurements.

NOMENCLATURE

Bi =Biot Number, $\frac{h_e t}{k}$

C = vane chord length = 56.2 cm

C_p = pressure coefficient, $\frac{p - p_\infty}{\frac{1}{2}\rho U^2}$

d =film cooling hole diameter = 4.1 mm

D_h = coolant channel hydraulic diameter

DR = coolant to mainstream density ratio

H = vane span height = 54.7 cm

I = film cooling momentum flux ratio

k = thermal conductivity

M = film cooling blowing ratio

p = static pressure, pitch between rib turbulators

Re = Reynolds number

s = streamwise surface distance from stagnation

t = thickness of vane wall = 1.27 cm

T = temperature

Tu = Turbulence Intensity

U = flow velocity

w = rib width

x = spanwise distance from film cooling hole

z =spanwise distance from bottom of vane

Greek

Λ_f = Turbulence integral length scale

η = adiabatic effectiveness

ϕ = Overall effectiveness

θ = non-dimensional temperature

ρ = density

ν = kinematic viscosity

Subscripts

0 = value with no film cooling

c = coolant at test vane coolant circuit inlet

C = true chord of airfoil

cc = conduction correction

e = external

f = film at film cooling exit

int = internal coolant

p = predicted value

w = outer wall surface

∞ = freestream

EXPERIMENTAL FACILITIES AND PROCEDURES

All experiments were conducted in a closed loop wind tunnel at the Unversity of Texas at Austin. The test section was a simulated three vane, two passage linear cascade. The vane geometry was the C3X vane of Hylton [8] scaled up 3.88 times. The center airfoil was removeable, which allowed for conducting and adiabatic airfoils to be interchanged in the test section. The test section featured two adjustable bypass flows and an adjustable outer wall designed to set the pressure distribution around the center test vane to that of an infinite cascade. A schematic of the test section is shown in Figure 1.

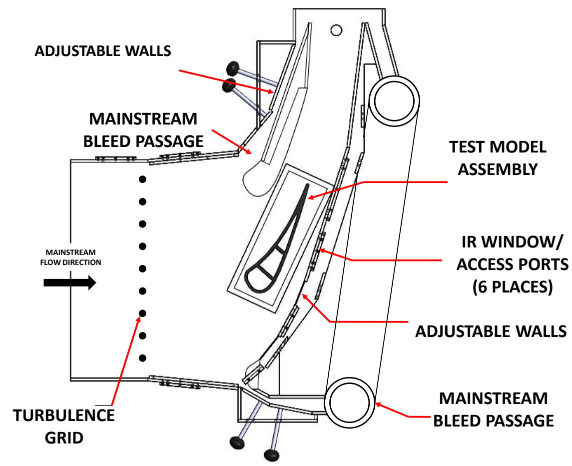

Figure 1: Schematic of the simulated turbine vane test section

The pressure distribution, measured and reported in a previous study, is shown in Figure 2. The pressure distribution was set by adjusting the external outer wall and bypass flows until the measured pressure distribution matched the CFD prediction of pressure for an infinite cascade. The scaled up vane had a true chord of C = 56.2 cm and a spanwise height of H = 54.7 cm. The pitch between vanes was 45.7 cm. The inlet approach velocity, U_∞, was set to 5.8 m/s which produced an exit Reynolds number based on true chord length of Re = 750,000. A removable passive turbulence generator grid was installed upstream of the test section and allowed for turbulence levels of Tu = 0.5% and Tu = 20% to be achieved. The integral length scales for the low and high freestream turbulence cases were measured to be Λ_f = 30 cm and Λ_f = 3 cm, respectively. The turbulence measurements were taken 0.26C upstream of the vane leading edge.

As mentioned previously, the test section was designed so that the center airfoil could be easily replaced. This allowed for both conducting (matched Bi) and near adiabatic vanes to be tested. The adiabatic test vane was constructed of low conductivity polyurethane foam with thermal conductivity k = 0.048 W/m*K. Implementing the matched Bi method requires that both Bi and the ratio of internal and external convective heat transfer coefficients be matched to the engine condition. In order to match Bi to the engine conditions, the conducting airfoil was constructed using a castable epoxy resin with thermal conductivity k = 1.02 W/m*K. Matching the ratio of internal to external heat transfer coefficients was achieved by designing an internal coolant flow circuit that could be adjusted across a wide range of coolant flow rates, allowing the ratio to be “dialed in” to the desired value. The internal coolant flow loop employed a U-bend channel to cool the leading edge region of the vane. A radial cooling channel was used to cool the middle portion of the vane. The trailing edge and aft regions of the vane were uncooled. A schematic of the internal coolant flow circuit is shown in Figure 3. Both the adiabatic and conducting vanes used the same internal coolant flow loop. Additionally, the internal flow loop used in the current study matches the geometry of Dees et al. [14-16]. More details on the design and geometry of the internal coolant circuit can be found in [14]. Where the work of Dees et al. [15] had rib turbulators installed in the internal coolant passages, the current work studies smooth internal walls.

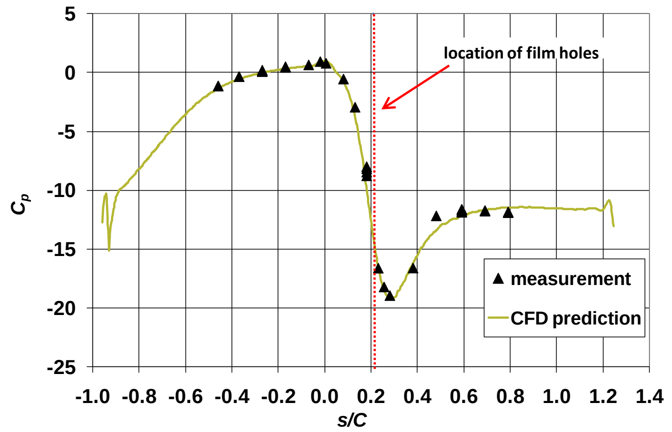

Figure 2: Test vane pressure distribution

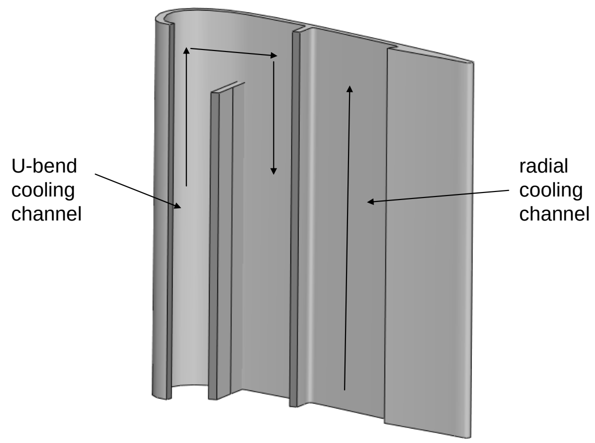

Figure 3: Test airfoil Schematic

In addition to internal coolant flow, test vanes used in the current study also had a row of film cooling holes on the suction side of the vane. A row of cylindrical film cooling holes were machined at s/C = 0.21. The diameter of the film cooling holes was 4.1 mm and the pitch to diameter spacing was *p/d* = 3. The film cooling holes had a streamwise injection angle of about $\alpha = 42°$. A schematic of the test vane showing the location of the suction side film cooling holes is shown in Figure 4. The as-built airfoil geometry is available via correspondence with the paper authors.

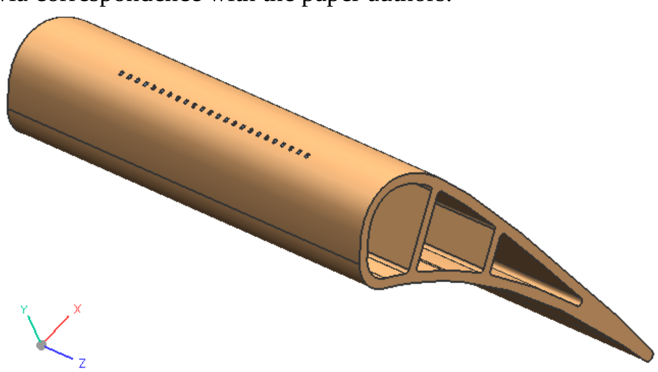

Figure 4: Suction Side Film Cooling Holes

The secondary flow loop was supplied to the test vane by bypassing some of the mainstream flow through a series of heat exchangers, flow control valves, and orifice meters. Liquid nitrogen was used to set the coolant temperature to the desired value. The flow control valves and flow meters were used to control the coolant flow rates through the U-bend and radial flow channels independently of each other. On the downstream side of the U-bend channel, which fed the suction side film cooling holes, a downstream control valve allowed for the pressure in the test vane to be adjusted. Adjustment of the pressure in the test vane allowed for the film cooling blowing ratio to be controlled independently of the flow through the U-bend circuit. A schematic of the secondary (coolant) flow loop can be seen in Figure 5.

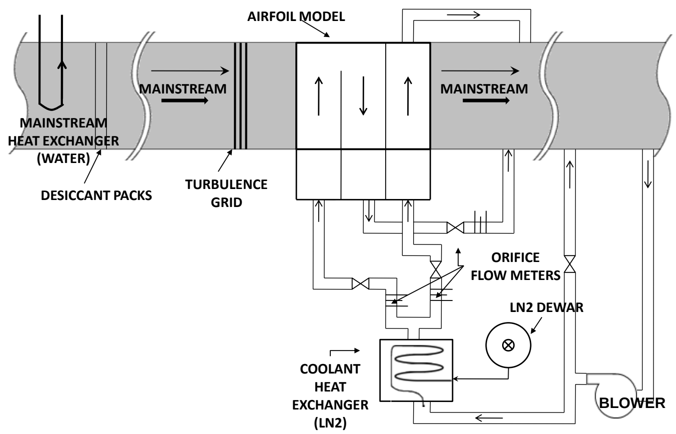

Figure 5: Schematic of secondary flow loop

Overall effectiveness measurements were obtained by installing the conducting airfoil into the test section. Surface temperature measurements upstream and downstream of the film cooling holes were taken using Flir P20 and P25 cameras simultaneously. Using two IR cameras simultaneously allowed for a larger region of the vane to be imaged in one test. Optical access to the test vanes was accomplished through two NaCl windows which could be installed into the test section sidewalls. Both cameras were calibrated during each test using E-type thermocouples attached to the vane surface in the field of view of the cameras. The entire surface was painted black to ensure a uniform surface emissivity. E-type thermocouples were also used to monitor the coolant temperature at the entrance to U-bend and radial coolant channels, the mainstream temperature, and the coolant temperature at the exit of the film cooling holes. The overall effectiveness was calculated using Equation 1

$$\phi = \frac{T_\infty - T_w}{T_\infty - T_c} \qquad (1)$$

In equation 1, the wall temperature (T_w) is normalized to the mainstream temperature (T_∞) and the coolant temperature at the inlet of the test airfoil (T_c).

For adiabatic effectiveness measurements the low conductivity foam vane was installed in the test section. Surface temperature measurements over the same region as the overall effectiveness measurements were taken using the same IR cameras. The cameras were calibrated for each adiabatic effectiveness test as well, although the camera calibration was found to be independent of the test vane conductivity. The adiabatic effectiveness values were calculated as shown in Equation 2.

$$\eta_{measured} = \frac{T_\infty - T_{aw}}{T_\infty - T_f} \tag{2}$$

In Equation 2, T_{aw} is the wall surface temperature measured on the adiabatic vane. The adiabatic effectiveness calculation differs from the overall effectiveness calculation in that the coolant temperature at the exit of the film cooling holes is used, rather than the coolant temperature at the inlet of the internal cooling circuit. For an adiabatic model, the coolant temperature at the inlet of the test vane and the coolant temperature at the exit of the film cooling holes should be the same value. Since the adiabatic vane was not truly adiabatic, there was some heat pickup between the vane inlet and the exit of the film cooling hole. This value was typically 1.0 to 1.5 K. On the conducting model, the increase in coolant temperature between the inlet to the test vane and exiting the film cooling holes was typically about 7K.

Since the adiabatic test vane was not truly adiabatic, the measured adiabatic effectiveness had to be corrected for conduction through the test vane material. In order to obtain an accurate measure of the necessary conduction correction, a separate experiment was performed. During this experiment the film cooling holes were smoothly taped over and the vane surface temperature was measured with only internal coolant flow present. The adiabatic effectiveness conduction correction reference value, η_{cc}, was subsequently determined from the measured surface temperature with no film cooling. Measured conduction correction values ranged between η_{cc} = 0.03 and 0.06. The conduction correction was then used along with the measured adiabatic effectiveness to calculate the corrected adiabatic effectiveness as shown in Equation 3. The derivation of Equation 3 can be found in Ethridge et al. [17].

$$\eta = \frac{\eta_{measured} - \eta_{cc}}{1 - \eta_{cc}} \tag{3}$$

Identical test conditions were used for overall effectiveness and adiabatic effectiveness measurements. In all cases the internal coolant flow Reynolds number, based on coolant channel hydraulic diameter, was Re = 20,000. The film cooling momentum flux ratio was tested at values of I = 0.34, 0.75, and 1.41. The coolant to mainstream density ratio was maintained at DR = 1.2 for all tests. This combination of blowing ratio and density ratio created blowing ratios of M = 0.64, 0.95, and 1.3. For a density ratio of DR = 1.2 and a nominal mainstream temperature of 300K, coolant temperatures were about 250 K. The coolant temperature used in the density ratio calculation was the coolant temperature at the exit of the film cooling holes, T_f. In order to eliminate the formation of frost in the secondary flow loop and on the vane surface, a procedure to dry out the wind tunnel was performed prior to each experiment. The drying procedure consisted of a gaseous nitrogen purge followed by installation of desiccant in the wind tunnel. This procedure produced relative humidity levels of less than 10% throughout the test, and was sufficient to eliminate frost concerns.

Precision uncertainty in overall and adiabatic effectiveness measurements was evaluated through a statistical analysis of the test to test repeatability of the data. Since the primary source of uncertainty for both measurements was the surface temperature measurement, and the surface temperature was measured in both cases using the same equipment, the statistical analysis was performed only on the overall effectiveness measurements and assumed to be representative of the adiabatic effectiveness measurements as well. The 95% confidence interval precision uncertainty, based on four independent test repeats, was calculated to be $\delta\phi = \delta\eta$ = ±0.02. The precision uncertainty in the measured conduction correction was determined to be about $\delta\eta_{CC}$ = ±0.02 through a similar analysis. The uncertainty in the conduction correction propagated to a bias uncertainty in the adiabatic effectiveness measurements of less than 0.01 at η = 0.6. Other bias uncertainties in the overall and adiabatic effectiveness measurements were made negligible by calibrating the thermocouples used in the experiments to the mainstream reference temperature.

RESULTS

The adiabatic effectiveness values downstream of the film cooling holes was measured over four film cooling hole pitches near the midspan of the airfoil for all three momentum flux ratios at the low freestream turbulence condition. Figure 6 presents laterally average adiabatic effectiveness values. The axis is normalized to the film cooling hole diameter, with the origin at the downstream of the film cooling hole breakout. As can be seen in the figure, the highest values of laterally averaged adiabatic effectiveness occur immediately downstream of film injection. Additionally, the lowest momentum flux ratio, I = 0.34, performed best over the whole test domain. Increasing the film cooling momentum flux ratio decreased the adiabatic effectiveness values. The decrease in adiabatic effectiveness with increased momentum flux ratio was attributed to coolant flow separation. On a flat plate, Thole et al. [18] showed that film cooling separation occurs for I > 0.4. Measurements on highly curved surfaces, by Ito et al. [19] and Schwarz et al. [20], present results for a similar film cooling geometry that show a peak in adiabatic effectiveness occurs near 0.4 < I < 0.5. The current results are consistent with trends previously shown in the literature.

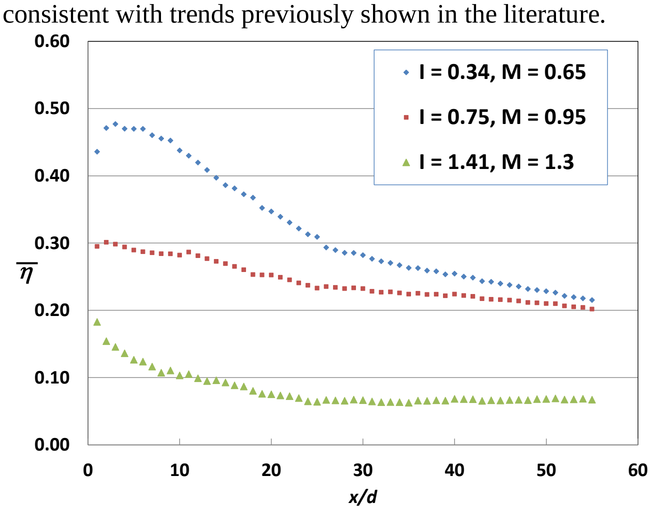

Figure 6: Laterally averaged adiabatic effectiveness measurements, *Tu* = 0.5%

Immediately downstream of film injection for I = 0.34, very high levels of adiabatic effectiveness were measured. The enhancement in film cooling performance on convex surfaces is due to normal pressure gradients that can pull attached film cooling jets toward the wall. Ito et al. [19] used a control volume analysis to show that for a convex surface film cooling performance will increase relative to a flat or concave surface for $I\cos^2\alpha < 1$, where α is the streamwise film cooling injection angle. Beyond this critical value of $I\cos^2\alpha$, film cooling performance actually decreases relative to flat or concave surfaces due to the normal pressure gradient being unable to compensate for the surface curving away from the trajectory of the jet. Additionally, the strength of the normal pressure gradient increases with decreasing radius of curvature, so more tightly curved convex surfaces experience more significant improvements in film cooling performance up to the critical value of momentum flux ratio. For the current study the curvature at film cooling injection has a value of $2r/d$ = 18, which is smaller than any curvature found in an existing open literature curved wall study. Smaller values of $2r/d$ indicate a more highly curved surface. Downstream of film injection, at x/d = 20 and x/d = 50, the surface curvature is increased to $2r/d$ = 79 and $2r/d \approx 10^{11}$, respectively. A flat plate has a radius of infinity, so the current airfoil clearly became more flat plate like with increasing x/d.

Figures 7 and 8 compare the film cooling performance at I = 0.34 and I = 0.75 with other film cooling studies on surfaces with varying curvatures at similar momentum flux ratios. These momentum flux ratios represent $I\cos^2\alpha$ = 0.25 and $I\cos^2\alpha$ = 0.56, so an improvement in film cooling performance relative to a flat plate should be seen in the current data. All of the studies used for comparison have film cooling geometries very similar to the current study. An improvement over the other curved surface results should also be seen, due to the smaller radius of curvature present in the current study. For I = 0.34, shown in Figure 7, the current study had higher adiabatic effectiveness values than any other study available for comparison other than Ito et al [19]. This was consistent with the current study having a significantly smaller radius of curvature than all other studies. In general, Figure 7 shows that decreasing the radius of curvature had the effect of increasing the adiabatic effectiveness for nominally the same coolant mass flux ratio. At I = 0.75, shown in Figure 8, similar trends were seen. The current study had a smaller radius of curvature at film injection and laterally averaged effectiveness values that were higher than all the measurements used for comparison purposes. As seen in Figure 7, decreasing the radius of curvature generally had the effect of increasing the laterally averaged adiabatic effectiveness.

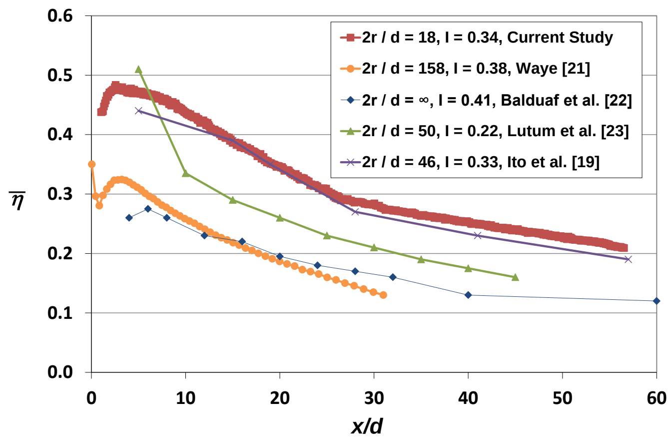

Figure 7: Effect of surface curvature on laterally averaged adiabatic effectiveness, *I* = 0.34, *Tu* = 0.5%

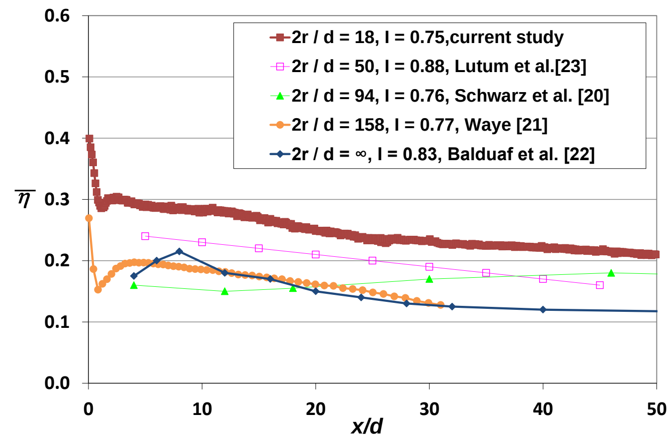

Figure 8: Effect of surface curvature on laterally averaged adiabatic effectiveness, *I* = 0.34, *Tu* = 0.5%

Contour plots of adiabatic effectiveness for all three momentum flux ratios are presented in Figure 9. Figure 9 shows that for all three momentum flux ratios the contours of adiabatic effectiveness values were asymmetric. This was likely due to the internal coolant crossflow feeding the coolant holes, which was about 2.3 m.s. A similar effect of internal crossflow on adiabatic effectiveness was seen by Gritsch et al. [24]. The effects of jet liftoff can be seen by comparing the three contour plots to each other. Figure 9b, which shows the adiabatic effectiveness values for I = 0.75, shows that the profiles of the film cooling on the surface were much thinner than those seen in Figure 9a, which show the adiabatic effectiveness levels for I = 0.34. For I = 1.41, shown in Figure 9c, the effect of jet detachment is even more pronounced. Only very thin regions of colder surface temperatures due to film cooling exist for I = 1.41.

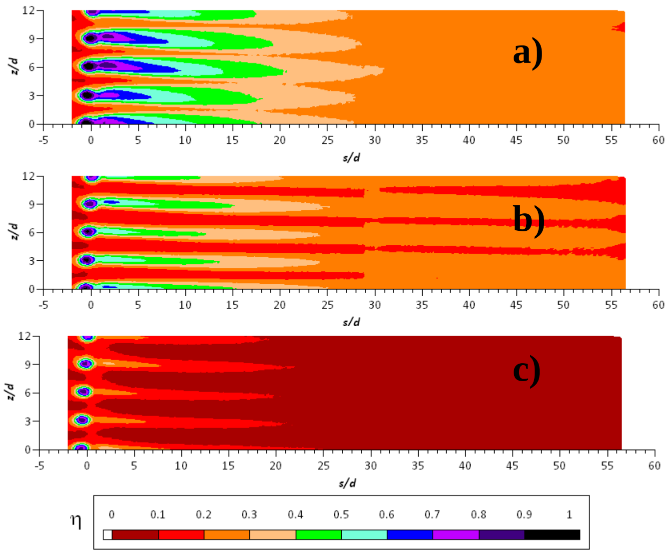

Figure 9: Contours of adiabatic effectiveness measurements, *Tu* = 0.5%, a) *I* = 0.34, b) *I* = 0.75, c) *I* = 1.41

Adiabatic effectiveness measurements were also measured for a high mainstream turbulence intensity of Tu = 20%. Figure 10 shows the laterally averaged adiabatic effectiveness values at both freestream turbulence levels. For I = 0.34 and I = 0.75, elevated freestream turbulence degraded the laterally averaged film effectiveness for x/d > 10. For both of these cases, the differences between the performance at Tu = 0.5% and Tu = 20% continues to grow with increasing downstream distance. At the end of the measurement domain, near x/d = 55, the laterally averaged overall effectiveness for both I = 0.34 and I = 0.75 was decreased by nearly 50% due to elevated Tu. For I = 1.41, no measurable differences in laterally averaged overall effectiveness due to the effect of freestream turbulence were seen.

Contours of adiabatic effectiveness at Tu = 20% are presented in Figure 11. For the two lowest momentum flux ratios, the high freestream turbulence caused the jets to merge earlier when compared to the low freestream turbulence cases shown in Figure 9. For the highest momentum flux ratio, the high freestream turbulence had the effect of increasing the mixing with the freestream and pulling some of the cold gas from the separated jet back down to the vane surface. This was evidenced than the wider jet footprint at the high freestream turbulence case relative to the low freestream turbulence case at the lack of a decrease due to high freestream turbulence in the laterally averaged adiabatic effectiveness measurements.

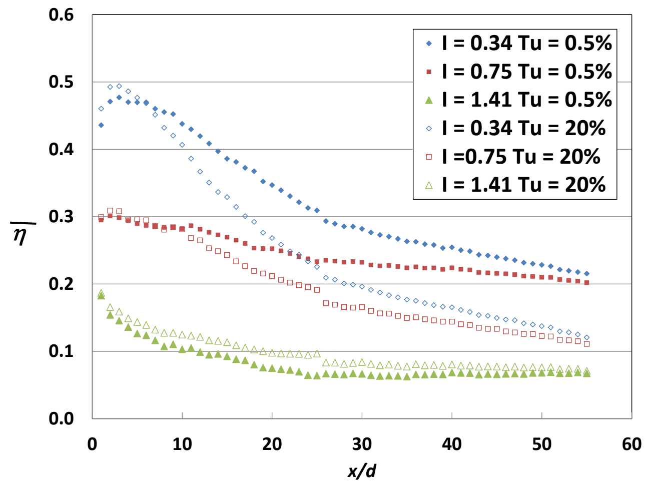

Figure 10: Laterally averaged adiabatic effectiveness measurements, *Tu* = 0.5% and 20%

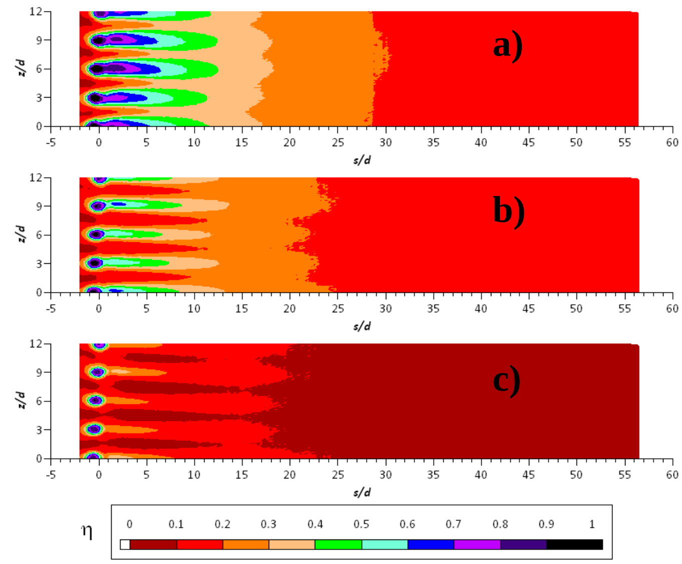

Figure 11: Contours of adiabatic effectiveness measurements, *Tu* = 20%, a) *I* = 0.34, b) *I* = 0.75, c) *I* = 1.41

Laterally averaged overall effectiveness values, measured on the Matched *Bi* test airfoil, are presented in Figure 12 for the same experimental conditions as the adiabatic effectiveness measurements. Figure 12 shows that as the momentum flux ratio increased the measured laterally averaged overall effectiveness values decreased. Of course, the film cooling is only one factor contributing to the overall cooling performance, or overall effectiveness. The internal convective cooling also was a significant contributor to the overall effectiveness on the vane. For all three momentum flux ratios, the coolant flow rate at the vane inlet was set at $Re_{ubend} = Re_{radial}$ = 20,000, which implies that the internal heat transfer was nominally the same for all three momentum flux ratios. Since the internal convective heat transfer was the same for all three cases, decreases in ϕ were expected where decreases in η were measured, consistent with the results shown in Figure 12.

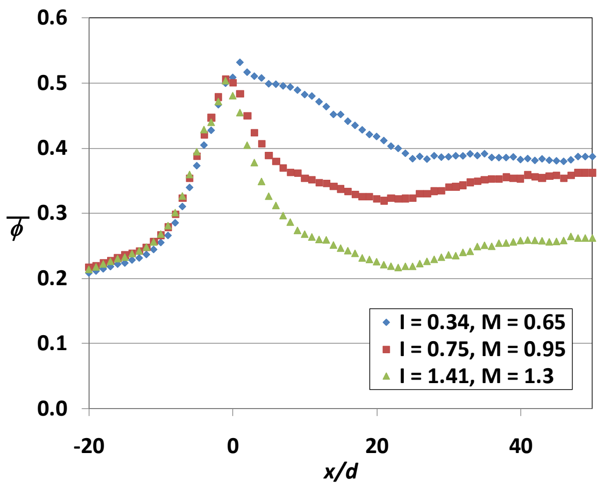

Figure 12: Laterally averaged overall effectiveness measurements, *Tu* = 0.5%

As shown in Figure 12, for $x/d > 20$ the values of overall effectiveness began to increase slightly with increasing downstream distance for both $I = 0.75$ and $I = 1.41$. The reason for this increase can be seen clearly in Figure 13. Figure 13 plots the same three laterally averaged overall effectiveness curves seen in Figure 12 along with overall effectiveness values for a non-film cooled surface with a tripped and non-tripped upstream boundary layer. The non-film cooled measurements were reported in Dees et al. [14]. The overall effectiveness values with no film cooling present were a result of the internal convective cooling only. The tripped upstream boundary layer was accomplished by placing a 1 mm boundary layer trip at $s/C = 0.2$, nominally the position of the film cooling holes. As can be seen in Figure 13, for $s/C > 0.4$, both the tripped and non-tripped non-film cooled overall effectiveness values were increasing with increasing downstream distance. When the adiabatic effectiveness approaches zero, the surface temperature distribution on the conducting model should approach the tripped, non-film cooled surface temperature distribution. The overall effectiveness should approach the tripped, non-film cooled overall effectiveness since film cooling injection acts as a boundary layer trip. This expectation is consistent with the results presented in Figure 13, particularly for $I = 1.41$, which had the lowest adiabatic effectiveness values far downstream of film injection.

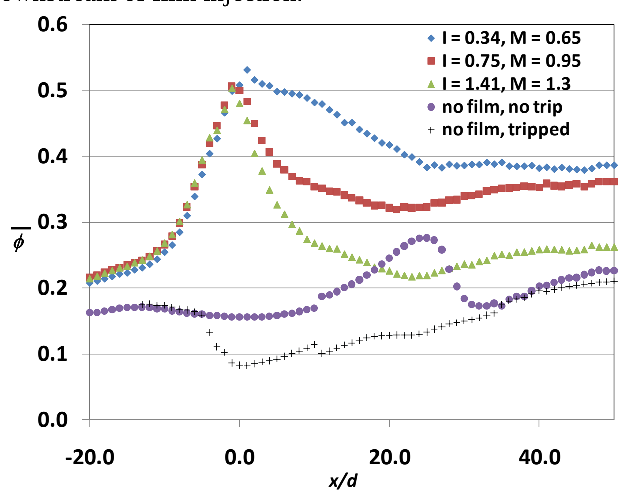

Figure 13: Laterally averaged overall effectiveness measurements with non-film cooled overall effectiveness measurements, *Tu* = 0.5%

Figure 13 is also useful in showing the relative contribution of the film cooling performance to the overall cooling scheme. As stated previously, overall effectiveness measurements without film cooling for a tripped and non tripped boundary layer are shown in Figure 13. These two non-film cooled reference cases were included to show the importance of the reference boundary layer state when evaluating film cooling performance. The non tripped, non-film cooled case is the appropriate baseline to use when evaluating the contribution of film cooling to the overall cooling performance since this temperature represents the vane temperature if no film cooling existed. In addition to lowering the gas temperature above the wall, film cooling has been shown to effectively trip otherwise laminar turbulent boundary layers at the film injection location. Harrison et al. [25] showed that film cooling caused as much as a 100% increase in external heat transfer coefficient relative to a non-tripped, non-film cooled surface and attributed to the increase to coolant injection tripping an otherwise laminar boundary layer. The effect of tripping the boundary layer and increasing the convective heat transfer coefficient is an undesirable side effect of film cooling and can offset the positive contributions of film cooling under certain conditions.

Figure 13 shows that in general the addition of film cooling increased the overall effectiveness relative to the non-tripped, non film cooled case. However, For $I = 1.41$ over the region $0.35 < s/C < 0.45$, the film cooled effectiveness was actually lower than the non-film cooled effectiveness. For this specific case the addition of film cooling was detrimental over the small region $0.32 < s/C < 0.43$ in terms of vane surface temperature. The augmentation in external heat transfer due increases in h due to film cooling was greater than the corresponding decrease heat transfer due to decreases in gas temperature above the wall, which ultimately caused a warmer surface temperature.

Comparing the overall effectiveness values to the tripped, non film cooled reference conditions allows for separation of the competing effects of heat transfer coefficient augmentation and reduced gas temperature due to film cooling. If the external heat transfer was nominally the same for all three momentum flux ratios and the no blowing case, which is suggested by Dees et al. [26], then any increase in overall effectiveness relative to the non film cooled, tripped case was attributable solely to the film cooling reducing the gas temperature above the vane surface. As can be seen in Figure 13, film cooling increased the overall effectiveness value relative to the tripped, non film cooled case everywhere.

In both Figures 12 and 13, an increase in the overall effectiveness upstream of the film cooling holes was measured. Figure 11 shows that a corresponding increase in overall effectiveness was not seen over the same region of the vane for the non film cooled models. This increase in overall effectiveness upstream of film injection on the film cooled model can be attributed to the convective heat transfer within the film cooling holes. These results show that the convective cooling within the holes caused noticeable cooling of the wall as much as 20 diameters upstream of the holes.

Using a 1-D analysis, the overall effectiveness on a film cooled wall can be shown to be equal to Equation 4, seen below.

$$\phi = \frac{1-\eta}{1+Bi+\frac{h_f}{h_c}} + \eta \tag{4}$$

Details on the derivation of Equation 4 can be found in Johnson et al. [27]. For a case where no film cooling is present and η is zero, Equation 4 can be simplified to produce Equation 5.

$$\phi_0 = \frac{1}{1+Bi+\frac{h_f}{h_c}} \tag{5}$$

Combining equations 4 and 5 produces Equation 6.

$$\phi_p = \phi_0(1-\eta)+\eta \tag{6}$$

Equation 6 can be used to predict the overall effectiveness, denoted with the subscript "p" in Equation 6, from measured adiabatic effectiveness values and non-film cooled overall effectiveness values. Figure 14 plots the measured overall effectiveness values with film cooling to predicted values calculated using Equation 6. The tripped, non-film cooled overall were used to calculate the predicted overall effectiveness values. As can be seen in Figure 14, for the I = 0.34 case, the predicted and measured overall effectiveness values agreed very closely. Agreement was also good for the I = 0.75 case, although not as good as what was seen at the lowest momentum flux ratio. Agreement between predicted and measured values was generally poor for the highest blowing ratio, which was likely fully detached from the vane surface. The results suggest that the ability to predict the overall effectiveness from the measured non-film cooled effectiveness and adiabatic effectiveness values depends on the level of jet detachment. For the low momentum flux ratio, where the jet was likely fully attached, the prediction and measurement agreed quite well. As momentum flux ratio increased, and the level of jet detachment presumably also increased, the agreement between the predicted and measured values worsened. Since the 1-D analysis used to develop Equation 6 relies on the assumption that the adiabatic wall temperature is the driving temperature for heat transfer to a film cooled wall, the results shown in Figure 14 would seem to suggest that for an attached jet this is a valid assumption. For detached jets, the assumption appears to becomes less valid as the level of jet detachment increases.

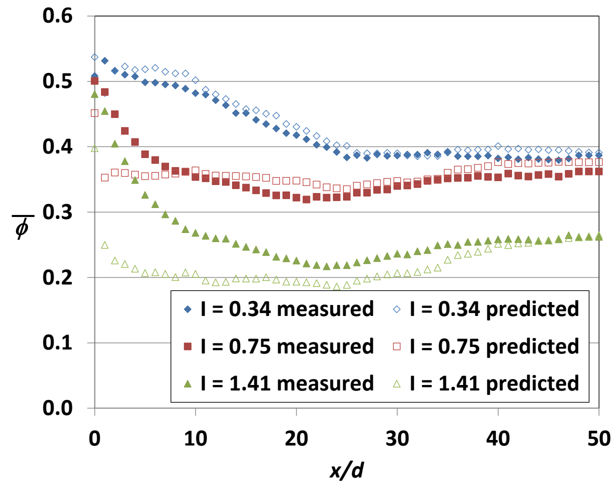

Figure 14: Measured and predicted laterally averaged overall effectiveness values, *Tu* = 0.5%

As was seen in Figure 9, the surface of the film cooled adiabatic wall had strong spanwise temperature variations. Figure 15 shows contours of overall effectiveness in order of increasing momentum flux ratio. As can be seen in all three overall effectiveness contour plots, the lateral conduction in the matched *Bi* model had the effect of drastically reducing the spanwise temperature gradients relative to the adiabatic case. Similar measurements of adiabatic and overall effectiveness on a simulated blade leading edge by Albert et al. [12] showed a similar reduction in spanwise temperature variations. As can be seen in Figure 15a, lateral conduction caused the "footprint" of the film cooling jets to disappear for x/d > 10 at I = 0.34. For I = 0.34 distinct jets could be seen in the contours of adiabatic effectiveness for x/d < 30, as shown in Figure 7. For the detached jets, I = 0.75 and I = 1.41, distinct contours in wall temperature corresponding to the location of the film cooling jets could not be distinguished in the overall contour plots.

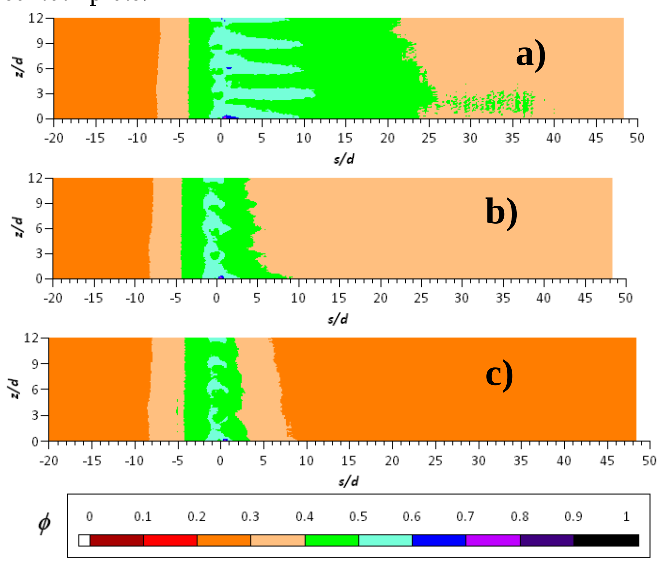

Figure 15: Contours of overall effectiveness measurements, *Tu* = 0.5%, a) *I* = 0.34, b) I = 0.75, c) *I* = 1.41

Figures 16 - 18 show the spanwise wall temperature variation on the surfaces of the conducting and adiabatic models at specific x/d locations. Figures 16 – 18 normalize the wall temperatures according to Equation 4.

$$\theta_w = \frac{T_\infty - T_w}{T_\infty - T_f} \tag{4}$$

This normalization uses the film temperature at the exit of the film holes as the normalization. For an adiabatic wall, Equation 3 is equivalent to adiabatic effectiveness.

Figure 16 shows the spanwise wall temperature variation for both models and all three momentum flux ratios at x/d = 1. For all three momentum flux ratios, spanwise temperature variations were much stronger on the surface of the adiabatic model, as was expected from inspection of the relevant contour plots. The influence of the internal conduction is evident for I = 1.41. For I = 1.41 the θ_w on the conducting wall was colder than the adiabatic wall everywhere due to the internal convection cooling the surface of the conducting model. For the I = 0.34 and I = 0.75 cases, the coldest temperatures at the jet centerline were equal to or colder for the adiabatic model than the conducting model.

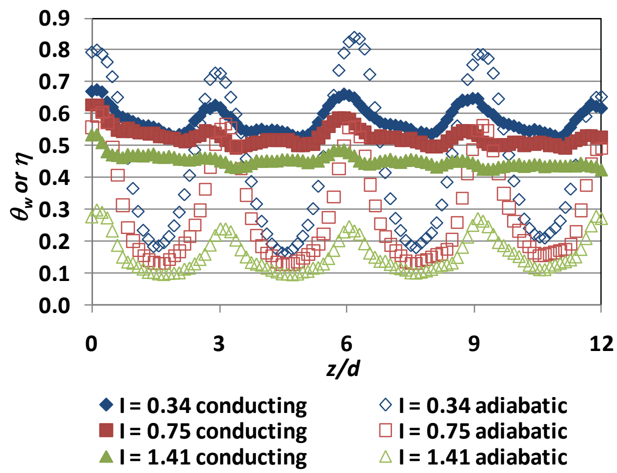

Figure 16: Spanwise variation in wall temperature, x/d = 1, Tu = 0.5%

At x/d = 10, shown in Figure 17, even smaller variations in surface temperature due to the film cooling jet can be seen on the conducting model. For I = 1.41 and I = 0.75, spanwise temperature variations were virtually nonexistent. On the adiabatic model, strong spanwise temperature variations were still present for all momentum flux ratios, but the variations were smaller than what were seen at x/d = 1. At x/d = 17, shown in Figure 18, streamwise temperature variations had decreased further on the conducting model relative to the upstream positions. However, slight spanwise temperature variations were still evident for the I = 0.75 conducting model case. For the adiabatic model, all variations in spanwise temperature were further reduced relative to x/d = 10. The strongest variations in spanwise temperature on the adiabatic model were seen in the I = 0.75 case, which may explain why spanwise variations were only seen on the conducting model at I = 0.75.

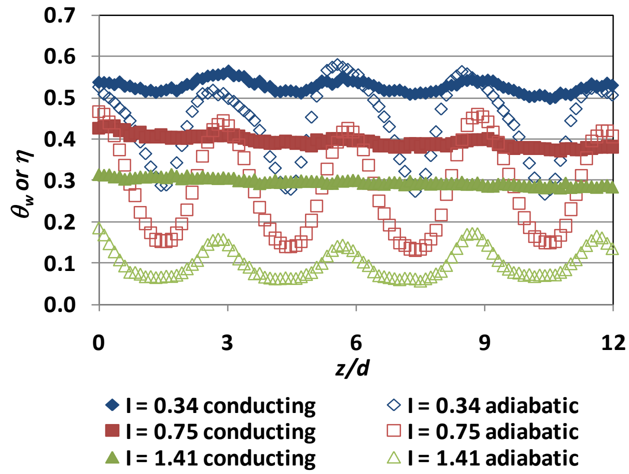

Figure 17: Spanwise variation in wall temperature, x/d = 10, Tu = 0.5%

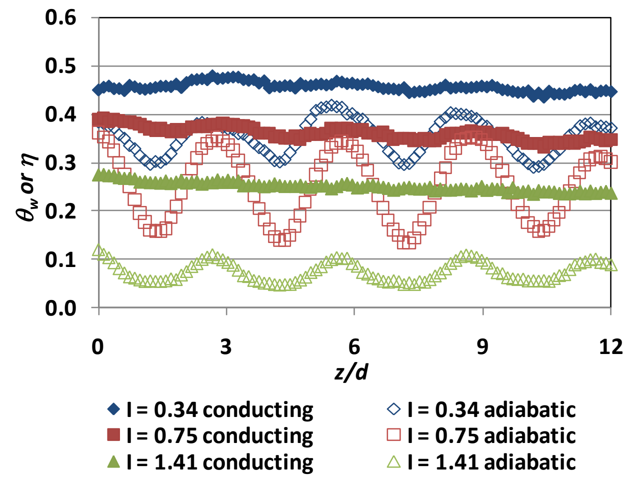

Figure 18: Spanwise variation in wall temperature, x/d = 19, Tu = 0.5%

CONCLUSIONS

This study presents surface temperature measurements downstream of a row of film cooling holes on the suction side of scaled up, simulated adiabatic and conducting gas turbine vanes. The overall and adiabatic effectiveness measurements presented in this study are the first parallel measurements made on adiabatic and conducting vanes with the same geometries and test conditions. In order to match non-dimensionalized surface temperatures representative of an engine component, the matched Bi model was used for the conducting vane.

The overall effectiveness measurements with film cooling compared to the overall effectiveness measurements without film cooling, measured in a previous study, allow for the contribution of film cooling to the overall cooling scheme to be separated from the contributions of the internal convective cooling. The current study showed that for nearly all conditions the addition of film cooling caused a decrease in vane surface temperature, as expected. However, over one small region of the vane at a high momentum flux ratio of I = 1.41, the addition of film cooling actually increased the vane surface temperature relative to the non-film cooled case. This was a result of the poor film cooling performance of the detached film cooling jet as well as an increased external heat transfer coefficient due to film cooling injection.

A significant goal of the current research was to provide an experimental benchmark for the validation of computational conjugate heat transfer codes. Previous experimental studies of conjugate heat transfer available in the open literature are limited in the scope of the data or were conducted on less realistic test models. Combined with previous studies by Dees et al. [7 – 9], the data presented in this paper represents a significant improvement in the experimental conjugate heat transfer data available for benchmarking of computational codes.

ACKNOWLEDGEMENTS

The authors gratefully acknowledge the support of the NASA NRA program for this research, and the guidance provided by the Technical Monitor Dr. J. Heidmann.

REFERENCES

[1] Harrison, K.L., and Bogard, D.G., 2010, “Use of the Adiabatic Wall Temperature in Film Cooling to Predict Wall Heat Flux and Temperature,” ASME paper GT2008-51424.

[2]Bohn, D.E., Ren, J., and Kusterer, K., 2003, “Conjugate Heat Transfer Analysis for Film Cooling Configurations with Different Hole Geometries,” ASME paper GT2003-38369.

[3]Kusterer, K., Bohn., D., Sugimoto, T., and Tanaka, R., 2006, “Conjugate Calculations for a Film-Cooled Blade Under Different Operating Conditions,” ASME paper GT2004-53719.

[4] Kusterer, K., Hagedorn, T., Bohn., D., Sugimoto, T., and Tanaka, R., 2006, “Improvement of a Film-Cooled Blade by Application of the Conjugate Calculation Technique,” *Journal of Turbomachinery*, vol. 128, pp572-578.

[5] Na, S., Williams, B., Dennis, R.A., Bryden, K.M., Shih, T. I-P., 2007, “Internal Film Cooling of a Flat Plate with Conjugate Heat Transfer,” ASME paper GT2007-27599.

[6] Shih, T. I-P., Chi, X., Bryden, K.M., Alsup, C., Dennis, R.A., 2009, “Effect of Biot Number on Temperature and Heat-Flux Distributions in a TBC-Coated Flat Plate Cooled by Rib-Enhanced Internal Cooling,” ASME paper GT2009-59726.

[7] Na, S., Dennis, R.A., Alsup, C., Bryden, K.M., and Shih, T.I-P., 2009, “Effect of Hot-Gas Composition on Temperature Distribution in a Flat Plate Cooled by Internal and Film Cooling,” ASME paper GT2009-59727.

[8] Hylton, L.D., Milhec, M.S., Turner, E.R., Nealy, D.A., and York, R.E., 1983, “Analytical and Experimental Evaluation of the Heat Transfer Distribution Over the Surface of Turbine Vanes,” NASA CR 168015.

[9] Turner, E.R., Wilson, M.D., Hylton, L.D., and Kaufman, R.M., 1985, “Analytical and Experimental Heat Transfer Distributions with Leading Edge Showerhead Film Cooling,” NASA CR 174827.

[10] Hylton, L.D., Nirmalan, V., Sultanian, B.K., and Kaufman, R.M., 1988, “The Effects of Leading Edge and Downstream Film Cooling on Turbine Vane Heat Transfer,” NASA CR 182133.

[11] Sweeney, P.C., and Rhodes, J.F., “An Infrared Technique for Evaluating Turbine Airfoil Cooling Designs,” *Journal of Turbomachinery*, vol. 122, pp 170 – 177.

[12] Albert, J.E., Bogard, D.G., and Cunha, F., 2004, “Adiabatic and Overall Effectiveness for a Film Cooled Blade,” ASME Paper GT2004-53998.

[13] Mouzon, B.D., Terrel, E.J., Albert, J.E., and Bogard, D.G., 2005, “Net Heat Flux Reduction and Overall Effectiveness for a Turbine Blade Leading Edge,” ASME paper GT2005-69002.

[14] Dees, J.E., Ledezma, G.A., Bogard, D.G., Laskowski, G.M., Tolpadi, A.K., 2010, “Experimental Measurements and Computational Predictions for an Internally Cooled Simulated Turbine Vane,” ASME paper IMECE2009-11622.

[15] Dees, J.E., Ledezma, G.A., Bogard, D.G., Laskowski, G.M., Tolpadi, A.K., 2010, “Experimental and Computational Measurements for an Internally Cooled Simulated Gas Turbine Vane with 90 degree Rib Turbulators,” ASME paper GT2010-23004.

[16] Dees, J.E., Ledezma, G.A., Bogard, D.G., Laskowski, G.M., Tolpadi, A.K., 2010, “Momentum and Thermal Boundary Layer Development on an Internally Cooled Turbine Vane,” ASME paper GT2010-23008.

[17] Ethridge, M.I., Cutbirth, J.M., and Bogard, D.G., 2001, “Scaling of Performance for Varying Density Ratio coolants on an airfoil with Strong Curvature and Pressure Gradient Effects,” *J. of Turbomachinery*, Vol. 123.

[18] Thole, K.A., Sinha, A., Bogard, D.G., and Crawford, M.E., 1992, “Mean Temperature Measurements of Jets with a Crossflow for Gas Turbine Film Cooling Application,” *Rotating Machinery Transport Phenomena*, edited by J.H. Kim and W.J. Wang, Hemisphere, New York, pp. 69 – 85.

[19] Ito, S., Goldstein, R.J., and Eckert, E.R.G., 1978, “Film Cooling of a Gas Turbine Blade,” *Journal of Engineering for Power*, vol. 100, pp. 476 – 481.

[20] Schwarz, S.G., Goldstein, R.J., and Eckert, E.R.G., 1990, “The Influence of Curvature on Film Cooling Performance,” ASME paper 90-GT-10.

[21] Waye, S.K., 2005, “Film Cooling Effectiveness of Suction Side Axial Holes, Compound Angle Holes, and Axial Holes Embedded within an Overlying Transverse Trench,” Master’s Thesis, The University of Texas at Austin.

[22] Balduaf, S., Scheurlen, M., Schulz, A., and Wittig, S., 2002, “Correlation of Film Cooling Effectiveness from Thermographic Measurements at Engine Like Conditions,” ASME paper GT2002-30180.

[23] Lutum, E., von Wolfersdorf, J., Weigand, B., and Semmler, K., 2000, “Film Cooling on a Convex Surface with Zero Pressure Gradient Flow,” *International Journal of Heat and Mass Transfer*, vol. 43, pp. 2973 – 2987.

[24] Gritsch, M., Schulz, A., Wittig, S., 2003, “Effect of Internal Coolant Crossflow on the Effectiveness of Shaped Film-Cooling Holes,” *Journal of Turbomachinery*, vol. 125, pp. 547 – 554.

[25] Harrison, K.L., Dorrington, J.R., Dees, J.E., Bogard, D.G, and Bunker, R.S., 2007, “Turbine Airfoil Net Heat Flux Reduction with Cylindrical Holes embedded in a Transverse Trench,” ASME Paper GT2007-27996.

[26] Dees, J.E., Bogard, D.G., and Bunker, R.S., 2010, “Heat Transfer Augmentation Downstream of Rows of Various Dimple Geometries on the Suction Side of a Gas Turbine Airfoil,” Journal of Turbomachinery, vol. 132.

[27] Johnson, R., Maikell, J., and Bogard,. D., 2009, "Experimental Study of the Effects of an Oscillating Approach Flow on Overall Cooling Performance of a Simulated Turbine Blade Leading Edge," ASME paper GT2009-60290.